Biol. Cybern. 62, 157–165 (1989)

Biological Cybernetics

Looking into the Water with a Facet Eye

D. Varjú and G. Horváth*

Lehrstuhl für Biokybernetik, Universität Tübingen, Auf der Morgenstelle 28, D-7400 Tübingen 1, Federal Republic of Germany

Abstract. The apparent velocity and apparent size of objects approaching an animal strongly depend on their size, their position within the visual field and on the path along which they move. It also makes a considerable difference whether both the animal and the objects are in air, or whether the animal looks from one medium into the other, as is the case in animals that live at the water surface. To systematically investigate this situation we calculated apparent velocity and size in the midsagittal plane of approaching objects of flat horizontal, rodlike vertical and spherical shape. We confine our investigation to object movements along straight horizontal and vertical paths and consider the situation for eyes with and without acute zones. The apparent velocity of an approaching object is low in the far field and increases rapidly close to the eye in both air and water. Along *horizontal* paths and close to the animal it is higher in water than in air. Along *vertical* paths and close to the animal it is higher in air than in water. Both relationships are exaggerated when there is an acute zone for vertical resolution along the animal's horizon. Boundary curves are calculated along which an approaching object is seen by a linearly increasing number of receptors. The change of apparent size is characterized by the density of these lines. Below the water surface the change of apparent size is similar to that of the apparent velocity. The apparent size of a horizontally elongated object approaching along a horizontal path increases steadily, that of a vertically elongated object along a vertical line initially increases, but can decrease again near the water surface. An acute zone substantially changes the shape and density of these contour lines. The biological consequences of these effects are discussed.

* Permanent address: Hungarian Academy of Sciences, Central Research Institute for Physics, Biophysical Group, P.O.B. 49, H-1525 Budapest, Hungary

1 Introduction

Animals like waterstriders or herons are confronted with the task to detect and locate objects under the water surface while looking into the water from the air. Due to refraction, the visual world under water is distorted. Waterstriders spend most of their time on the ideally flat water surface; consequently, different parts of their eyes always see similar patterns. The dorsal part looks into the sky, the equatorial region sees the shores and objects on the water surface, and the ventral part looks into the water. We do not know much about the tasks the different parts of the eye perform. There are differences in the structure of the rhabdoms (Schneider and Langer 1969; Wohlburg-Buchholz 1979). Prey producing surface waves are readily localized by means of mechanosensors in the legs too (Liche 1936; Murphey 1971), but at least in capturing the prey on the water surface vision plays an important role (Liche 1936).

Gerris is said to feed also on aquatic insect larvae, which are captured while approaching the surface for breathing (Günther 1968). According to our own observations, Gerridae are attacked from below e.g. by the backswimmer *Notonecta*. It is not known to us whether approaching mosquito larvae or *Notonecta* produce waves which can be utilized by *Gerris*. It is possible that *Gerris* has to rely on vision in order to detect and locate both prey and predator below the water surface. Thus, we think it is an interesting question what waterstriders see when looking into the water. In this study we confine ourself to the question of detecting underwater objects of different sizes and shapes. The answer might reveal to what extent a facet eye is principally suited to perform these above tasks. Our hypothesis is that the apparent velocity and the change of apparent size might be the relevant parameters for detection of an approaching object.

2 Methods

The predator *Notonecta* usually approaches Gerridae along a path immediately below and parallel to the water surface. Mosquito larvae rise along a path vertical to the water surface. Having the possible prey and predators of *Gerris* in mind we restrict our calculations first to flat horizontal and rodlike vertical objects moving along horizontal and vertical paths in the mid-saggittal plane below the animal. For comparison we consider also spherical objects. In a vertical plane these objects are represented by horizontal and vertical lines with length L and height H, and by a circle with radius r, respectively.

When an object moves across the visual field the number of ommatidia crossed per second is taken as a measure of the apparent velocity, the number of ommatidia covered by the object as a measure of apparent size. The variables we calculate first are the horizontal and vertical distances Dx and Dy between the optical axes of the ommatidia in the midsagittal plane along horizontal and vertical paths below the horizon. Assuming that a pointlike object such as the rostral end of an approaching backswimmer or larva moves with uniform velocity, the apparent velocities v_x and v_y, that is the number of optical axes crossed per second will be proportional to 1/Dx and 1/Dy.

To characterize the apparent size of an object we calculate boundary lines along which the object covers a given number of ommatidia.

The spatial resolution of a facet eye is determined by the interommatidial angle Φ between the axes of neighbouring ommatidia. As a first step we assumed that this angle is constant across the visual field. We choose $\Phi = 4°$, which is about the average interommatidial angle in the ventral part of the eye of *Gerris*. Yet it is well established that animals living in a flat environment have horizontally aligned acute zones. This means that the interommatidial angle is narrow along the eye equator and increases towards the dorsal and ventral visual field (Zeil et al. 1986, 1989). This is also the case in waterstriders (Dahmen and Junger 1988). Thus in addition we compute the apparent velocities and the lines of constant apparent size also with varying interommatidial angles. We used an approximation which roughly corresponds to the eye of *Gerris* (inset in Fig. 5c, Dahmen and Junger 1988; Dahmen, personal communication).

The equations used are derived in the Appendix.

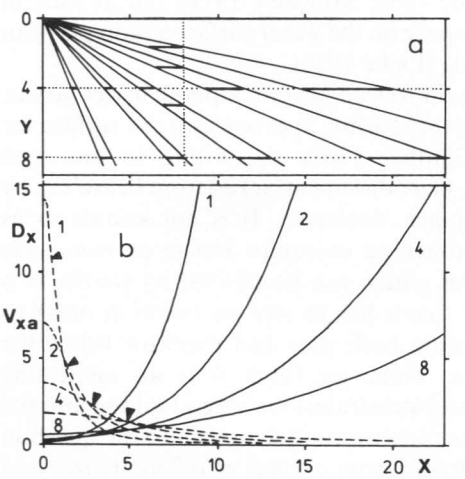

Fig. 1. a Variation of the distance Dx between the border lines of adjacent ommatidia along horizontal lines with variing distances x and y in air (arbitrary units). **b** Quantitative relationships between Dx (solid lines) as well as $v_{xa} = 1/\mathrm{D}x$ (dashed lines) and x, with y as parameter. v_{xa} is taken as a measure of the apparent velocity, arrowheads mark the maximum of its change, i.e. the highest acceleration. The interommatidial angle is $\Phi = 4°$

3 Results

3.1 The Apparent Velocity of Objects Moving Along Horizontal and Vertical Paths

We confine our consideration mostly to areas not too far away from the animal because *i)* the events we are considering are important for an insect primarily within these areas, and *ii)* the variables we are dealing with show interesting changes also mainly within this range. The eye is always thought to be at the origin of the $x-y$ coordinate system (Fig. 13).

In Fig. 1a we illustrate how Dx changes along a horizontal line at different distances y below the eye in air. The interommatidial angle amounts to 4°. In Fig. 1b Dx is plotted over x with y as parameter (solid lines). It decreases with decreasing x and increasing y. The dashed curves show the apparent velocity $v_{xa} = 1/\mathrm{D}x_a$. Due to symmetry, Dy can be derived when x and y are interchanged in the denominator of (1). Thus the curves in Fig. 1 apply also to Dy and $v_{ya} = 1/\mathrm{D}y_a$.

The apparent speed of an object moving with uniform velocity along a horizontal or vertical path increases strongly the closer it comes to the eye, and decreases asymptotically to zero with increasing distance. The highest apparent velocities are observed close to the eye (dashed line labeled 1).

The change of the apparent velocity might be another parameter the animals could use to detect an object. To characterize its variation with the parameter of the path along which an object approaches we marked its maximum with arrowheads along the velocity curves. This maximum shifts to higher coordinate values as the path parameter increases, but at the same time its value diminishes.

In Fig. 2a we demonstrate in a qualitative manner how the situation changes when the animal looks from

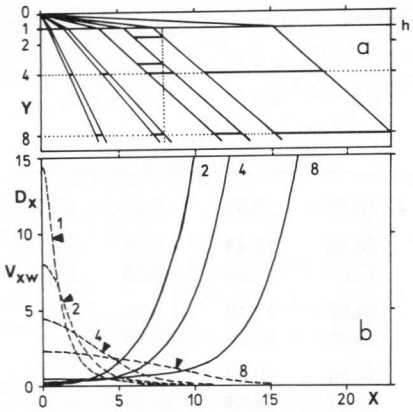

Fig. 2a and b. The same relationships as in Fig. 1 but under the water surface. The water surface is at $y=h$ below the eye. Here and in all following diagrams distances are given as multiples of h

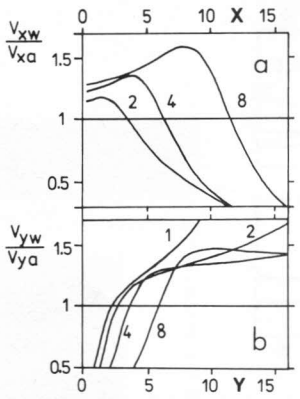

Fig. 4. **a** The relationship v_{xw}/v_{xa} for an object moving along horizontal paths versus x with y as parameter. **b** The relationship v_{yw}/v_{ya} for an object moving along vertical paths, with parameter x (cf. Figs. 2 and 3)

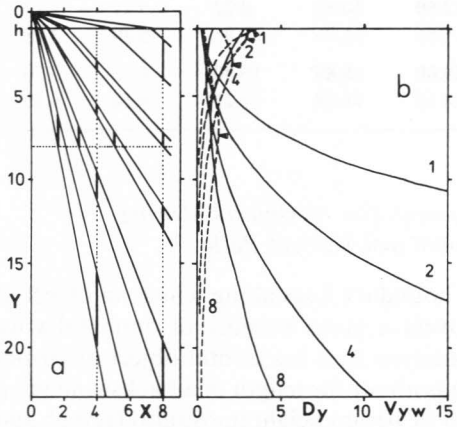

Fig. 3a and b. Similar diagrams as in Fig. 2, but now to illustrate the variation of the distance Dy along vertical lines (**a**) and to show Dy as well as $v_{yw}=1/\mathrm{D}y$ versus y (**b**) with x as parameter

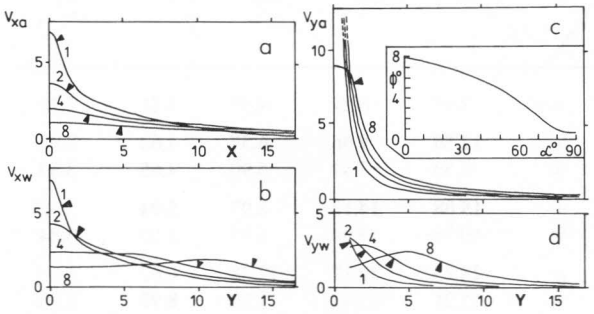

Fig. 5a–d. Same relationships as in Figs. 1b–3b, but now the interommatidial angle varies according to the function shown in the inset of **c**

air into water with the eye at height h above the surface. To calculate Dx we first have to reconstruct the path of a ray which originates at a point (x, y) and arrives, after refraction, at the eye. The formulae used for these calculations are (6)–(9). All distances are given as multiples of h.

Having established the angle α (Fig. 13b), the horizontal distance between the optical axes of neighbouring ommatidia after refraction can be calculated from (4). The results are presented in Fig. 2b. Although $\mathrm{D}x_w$ and $v_{xw}=1/\mathrm{D}x_w$ are similar to the corresponding variables in Fig. 1b, interesting quantitative differences become apparent, when we calculate e.g. the ratio v_{xw}/v_{xa} (Fig. 4a).

In water the results along vertical lines differ from those along horizontal lines (cf. Figs. 2a and 3a). There is a qualitative difference between air and water. When x becomes larger, the apparent velocity first increases and then decreases again, as the object approaches the water surface (Fig. 3b, curves labeled 4 and 8). This difference becomes more apparent by plotting the ratio v_{yw}/v_{ya} (Fig. 4b).

When we take a variable interommatidial angle Φ over α into consideration (cf. inset Fig. 5c), both the velocity profiles (Fig. 5) and the ratios v_{xw}/v_{xa}, v_{yw}/v_{ya} (Fig. 6) change considerably. Along horizontal paths the apparent velocity becomes higher in the far and lower in the near field in both air and water (Fig. 5a and b). Since the resolution increases towards the horizon, the apparent velocity along vertical paths is considerably higher near the animal than with uniform resolution (Fig. 5c and d), as the object approaches the horizon in air respectively the surface in water.

Since the apparent velocity might be the relevant parameter for the detection of objects we calculated the distances along different paths at which the perceived

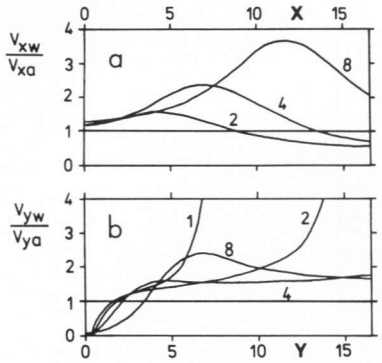

Fig. 6a and b. Same relationships as in Fig. 4 with varying interommatidial angle

Table 1. Distances d along horizontal (upper half) and vertical lines (lower half) at which the perceived velocity reaches arbitrarily chosen threshold values v^* (rel units) in air (a) respectively in water (w). Larger values boldfaced. "----": value not reached. $\Phi = 4°$

d	v^*	0.1	0.2	0.5	1	2
1	a, w	7.93	6.27	4.37	3.21	2.28
2	a	**12.50**	**9.56**	**6.37**	4.62	2.97
	w	9.53	7.87	5.90	**4.65**	**3.53**
4	a	**19.08**	**14.13**	**8.97**	**5.94**	3.32
	w	10.78	9.04	6.97	5.50	**3.84**
8	a	**28.23**	**20.17**	**12.38**	6.62	----
	w	15.21	13.42	11.08	**8.95**	2.92
1	a	7.93	6.27	4.32	3.21	2.28
	w	**9.34**	**7.22**	**4.86**	**3.44**	**3.21**
2	a	12.50	9.56	6.37	4.62	2.97
	w	**14.78**	**11.10**	**7.28**	**5.05**	**3.21**
4	a	19.08	14.13	8.97	5.94	3.32
	w	**22.58**	**6.58**	**11.08**	**7.12**	----
8	a	28.23	20.17	12.38	6.62	----
	w	**33.50**	**24.13**	**14.92**	**9.51**	----

velocity reaches arbitrarily selected values (v^*). The results are presented in Table 1. An object approaching along horizontal lines reaches a low threshold v^* earlier in air, higher ones earlier in water. Along vertical lines all thresholds will be reached, if at all, earlier in water.

Taking variable Φ into account the distance at which the perceived velocity rises over the threshold will be increased considerably along horizontal lines (Table 2, upper half). The apparent velocity reaches the threshold values in most cases also along vertical lines earlier in air than in water.

Table 2. Same as in Table 1, Φ varies as shown in the inset of Fig. 5c

d	v^*	0.1	0.2	0.5	1	2
1	a, w	22.20	16.57	10.93	7.66	4.27
2	a	**33.13**	**24.28**	**15.45**	8.55	2.68
	w	23.33	17.67	12.04	**8.75**	**5.17**
4	a	**48.50**	**34.60**	**17.10**	5.34	----
	w	25.60	19.96	14.29	**10.93**	----
8	a	**69.50**	**44.00**	10.67	----	----
	w	30.10	24.64	**18.75**	15.30	----
1	a	**14.80**	**8.97**	**4.90**	**3.19**	**2.07**
	w	5.88	4.73	3.31	2.39	1.56
2	a	**18.00**	**11.29**	**6.34**	**4.12**	**2.61**
	w	9.78	7.61	5.19	3.71	2.40
4	a	**22.50**	**14.55**	**8.22**	5.21	3.14
	w	15.56	11.86	7.95	**5.70**	**3.75**
8	a	**29.00**	**18.89**	10.40	6.26	3.70
	w	24.10	18.08	**12.21**	**9.10**	**6.40**

3.2 The Apparent Size of Objects Moving along Horizontal and Vertical Paths

To calculate boundary lines along which an object of given size covers a given number of ommatidia we restrict our analysis to a horizontal object of 20 mm length, which is about the length of a backswimmer, a vertical object of 10 mm height (mosquito larvae), and a sphere of 3 mm radius. The latter roughly corresponds to small-sized species of the water beetle families Haliplidae and Hydrophylidae, which also approach the surface and might be potential prey. The change of apparent size along any path can be derived from the calculated boundary lines. The height h of the eye above the water surface is 2–3 mm in waterstriders. Since we chose h as the unit of distance, we used the size parameters 10, 5, and 1.5 in the calculations. The results are shown in Figs. 7–9 for a constant, and in Figs. 10–12 for varying interommatidial angle.

Size can be perceived only when an object covers at least one ommatidium. When the proximal end of an elongated object of given length or the centre of a spherical object of given radius comes to lie on the boundary lines labeled 1 in Figs. 7–12, it then covers just one ommatidium. We call the area enclosed by this line and the coordinate axes the area of detectability (AOD), since an object of given size cannot be detected by means of apparent size change outside of this area. The object can, of course, be detected if it moves around and crosses the border lines between ommatidia.

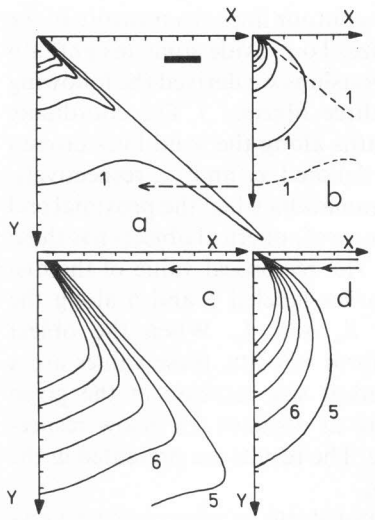

Fig. 7a–d. Boundary lines along which a flat horizontal object (bar) of length $L=10h$ covers a given number of ommatidia starting with 1 (outermost curves) in water (**a**) and in air (**b**). The outermost curve in **a** is reproduced also in **b** for better comparison (dashed curve labeled 1). Step size: 1. **c** and **d** are enlarged version of **a** and **b**. Along the outermost curve the object covers 5 ommatidia. The horizontal line below the x-axis represents the water surface at $y=h$, which is shown for comparison also in the diagrams for air. The distance between the divisions along the axes is $20h$ in **a** and **b**, $2h$ in **c** and **d**. An object moving along the dashed straight line reaches and leaves the area enclosed by the boundary line labeled 1. The solid lines with arrowheads are selected paths to derive parameters described in the text and given in Tables 1 and 2. Uniform resolution

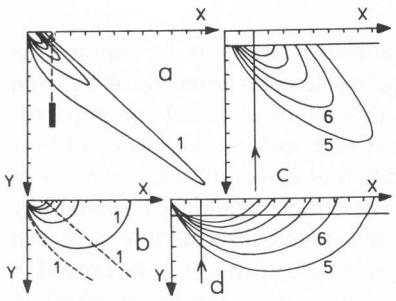

Fig. 8a–d. Boundary lines for a rodlike vertical object (bar) of height $H=5h$. Same conventions as in Fig. 7. The distance between the divisions along the axes is $10h$ in **a** and **b**, h in **c** and **d**. Uniform resolution

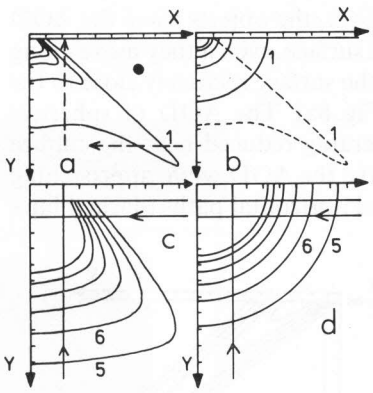

Fig. 9a–d. Boundary lines for a spherical object (filled circle) of radius $r=1.5h$. Same conventions as in Fig. 7. The distance between the divisions along the axes is $10h$ in **a** and **b**, h in **c** and **d**. Uniform resolution

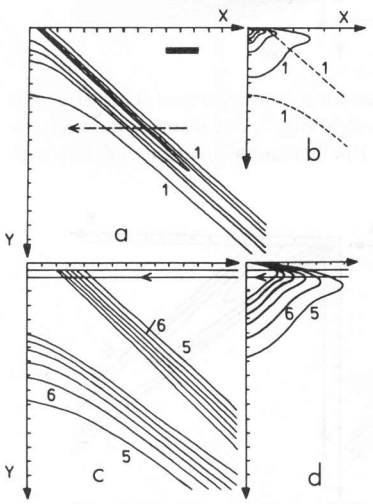

Fig. 10a–d. Boundary lines for a horizontal object (bar) of length $L=10h$. Same conventions as in Fig. 7. The distance between the divisions along the axes is $20h$ in **a** and **b**, $2h$ in **c** and **d**. Eye with acute zone

For an eye with uniform resolution the contour lines in air are circles (Figs. 7b and d–9b and d, see Appendix for derivation). When an elongated horizontal object approaches along a horizontal path in air, it remains within its AOD after reaching an angular extension larger then Φ (Fig. 7b and d). The same is true for an elongated vertical object moving along vertical paths (Fig. 8b and d), and for spherical objects approaching along both horizontal and vertical straight paths (Fig. 9b and d).

In water the contour lines are no longer circles (Figs. 7a and c–9a and c). For flat horizontal objects moving along horizontal paths there is little difference between air and water (Fig. 7). The AOD is somewhat reduced near the surface and increased at greater depth (compare the dashed and solid curves labeled 1 in Fig. 7b). At larger depth, however, such as along the dashed line in Fig. 7a, the approaching object leaves again its AOD after crossing the same curve for a second time. There is a remarkable difference between air and water for vertical objects moving along vertical lines (Fig. 8). The AOD is reduced to a narrow

elongated area. Moreover, the objects leave the AOD while approaching the surface, even if they move along a path that intersects the surface relatively close to the eye (dashed line in Fig. 8a). The AOD of spherical objects is also considerably reduced near the surface (Fig. 9a). They can leave the AOD while approaching along both vertical and horizontal paths (dashed lines in Fig. 9a).

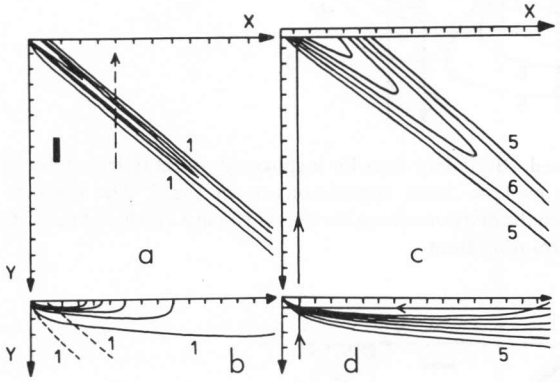

Fig. 11a–d. Boundary lines for a vertical object (bar) of height $H = 5h$. Same conventions as in Fig. 7. The distance between the divisions along the axes is $10h$ in **a** and **b**, $2h$ in **c** and **d**. Eye with acute zone

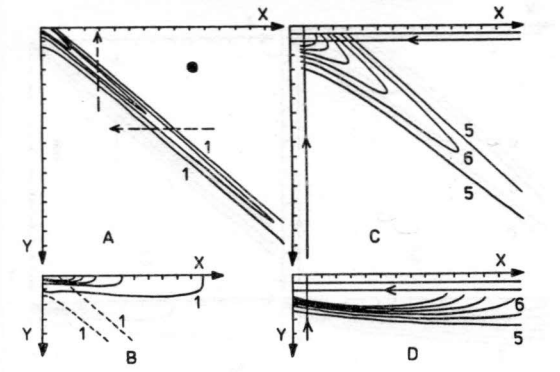

Fig. 12a–d. Boundary lines for a spherical object (filled circle) with radius $r = 1.5h$. Same conventions as in Fig. 7. The distance between the divisions along the axes is $10h$ in **a** and **b**, $2h$ in **c** and **d**. Eye with acute zone

The density of the contour lines is a measure of the change of apparent size. To provide some insight into the quantitative relationships we derived the following parameters for our three objects: *1* The coordinate value at which the paths along the solid lines crosses the curves labeled 5, denoted x_5 and y_5, respectively. The object covers 5 ommatidia when the proximal end of elongated or the centre of spherical objects has these coordinate values. *2* The reciprocal value of the distance between the curves labeled 5 and 6 along the same lines, denoted d_x and d_y. When the object approaches with uniform velocity, these values are a measure of the apparent size increase at the given position. The lines are at distance 2 h below respectively ahead of the eye. The results are presented in the upper half of Table 3.

Figures 10–12 demonstrate to what extent a varying interommatidial angle influences the shape of the AOD. In this case the boundary lines also in air are no longer circles, and there are considerable differences between air and water. The boundary lines in water enclose now narrow elongated areas in all three cases. Consequently, objects moving towards the animal along either horizontal or vertical paths at a given distance below the surface or ahead of the animal will leave the AOD (dashed lines). Along the same lines the apparent size first increases, but rapidly decreases again. Here, too, we derived the parameters x_5, y_5, d_x, d_y, which are presented in the lower half of Table 3.

4 Discussion

The aim of our theoretical study is to explore the geometry of the visual world of an animal looking from air into water. For this we determined the apparent velocity, the apparent size and its change for objects approaching from different direction. Our hypothesis is that these parameters might enable an animal like the waterstrider to detect and discriminate prey and predator. This analysis might turn out to be crucial in the seurch for the neural mechanisms involved in

Table 3. Parameter values in units of h to characterize the apparent size and its change in air and in water of three different objects. Upper two lines: $\Phi = 4°$; lower two lines: Φ varies with α. Conventions as in Table 1

	Horizontal		Vertical			Sphere		
	x_5	d_x	y_5	d_y	x_5	d_x	y_5	d_y
Air	**3.71**	1.75	2.93	**2.23**	**8.50**	0.64	8.50	**0.64**
Water	3.14	**2.33**	**3.43**	1.75	4.64	**2.33**	**11.21**	0.50
Air	**12.00**	0.52	1.71	**3.57**	**43.43**	0.13	5.29	**1.54**
Water	9.00	**0.93**	**2.00**	2.33	8.93	**1.00**	**6.07**	1.08

making these distinctions and for the interpretation of visual systems design (cf. Schwind 1980; Zeil et al. 1986, 1989; Nalbach and Nalbach 1987; Horváth 1989). We restricted our study to flat horizontal objects moving along horizontal paths and to rodlike vertical objects approaching along vertical paths below the water surface, since such objects are known predators and preys of *Gerris*. For comparison we also considered spherical objects moving along horizontal and vertical paths. Our considerations might also be relevant for animals and objects in air, for example for insects sitting on the stem of a plant, and for the special case of animals living on a flat substrate (cf. Zeil et al. 1986).

Essential for the animal is whether the apparent velocity and/or size of an approaching object will be detected at a sufficiently large distance so that there is enough time to respond appropriately. In this respect the situation is quite different for the different classes of objects considered. Horizontal objects approaching along horizontal paths reach the highest apparent velocities near the horizon in air or the water surfaces in water (Fig. 5a and b) but at a distance which would allow too little time for a reaction in case of fast objects. Similar considerations hold also for the apparent size and its increase (Figs. 7 and 10). At increasing distance below the surface threshold values for apparent velocities (Tables 1 and 2) and apparent size are reached at larger horizontal distances, and the change of both apparent velocity and size becomes slower. In this respect, the situation in water is less favorable than in air (Tables 1–3). Considering objects approaching along vertical paths we find for small values of x similar results as along horizontal paths. For large values of x the apparent velocity (Fig. 5c and d) and size (Figs. 8 and 11) first increase and decrease again near the water surface. Moreover, for an eye with uniform resolution threshold values of the apparent velocity occure at larger distances below the water surface than in air (Table 1, lower half).

Acute zones for vertical resolution at the horizon has been discussed as an improvement of distance perception in a flat word (Zeil et al. 1986, 1989). When we assume that it is important for waterstriders to detect its potential predator *Notonecta* in a sufficiently large distance either by means of the perceived velocity or of apparent size increase, then narrow interommatidial angles near the horizon are an advantage: The threshold distance is considerably larger with acute zones (Table 2, upper half) than with uniform resolution (Table 1, upper half). Similar relationships hold for the apparent size (Table 3, first column).

The detectability of approaching objects depends on *i)* their path direction relative to the animal, *ii)* environmental geometry, *iii)* the sampling pattern (uniform/acute zone), *iv)* threshold. Reducing the interommatidial angle near the horizon has the inevitable consequence that it will be increased in the ventral part of the eye, if number of ommatidia and/or the size of the eye cannot be increased. One might expect, therefore, that the detectability of objects approaching along vertical paths will be severly impaired. There is indeed some impairment, but the balance seems to be positive. Consider for example the columns below 0.2 and lines $2w$ in Tables 1 and 2. The threshold distance along the horizontal path is increased according the ratio $17.67 : 7.87 = 2.25$, whilst that along the vertical path reduced only as $7.61 : 11.1 = 1/1.46$. Similar relationships are true also for other parameter values. We obtain comparable results with respect to the distance at which an object has a certain apparent size. In Table 3 we find the ratio $9 : 3.14 = 2.87$ along the horizontal line (column x_5), whilst the ratio along the vertical line amounts to $2 : 3.42 = 1/1.71$ (column y_5). And, after all, detecting an attacking backswimmer in time is more important than detecting an approaching mosquito larva.

We touched so far only a few aspects of the properties and consequences of the geometry of the visual space in facet-eyed animals. Our conclusions are rather general and exemplary at the same time. The formalism we developed can, however, easily be adopted to analyze specific situations, i.e. cases where object size and path, as well as the distribution of interommatidial angle correspond to a given situation of an animal. The analysis is certainly worth to be extended. In the three dimensional space, for example, the apparent size of an approaching object increases also in the transverse plane and, depending on the distribution of the interommatidial angle, in different manner along different radii. The differences might enable the animal to identify the object. Similarly, if localization is required besides detection, depth perception and therefore possible binocular interaction and motion parallax might be of importance although localization in a predictable environment can be achieved without stereopsis (Zeil et al. 1986, 1989). These questions will be the subject of forthcoming investigations.

Appendix

In air the following relationships hold for the horizontal and vertical distances Dx, Dy between the optical axes of neighbouring ommatidia diverging by the angle Φ (Fig. 13a):

$$x/y = \mathrm{tg}\alpha;\ (x + Dx)/y = \mathrm{tg}(\alpha + \Phi), \tag{1}$$

resulting in

$$Dx = \mathrm{tg}\Phi(x^2 + y^2)/(-x\,\mathrm{tg}\Phi + y). \tag{2}$$

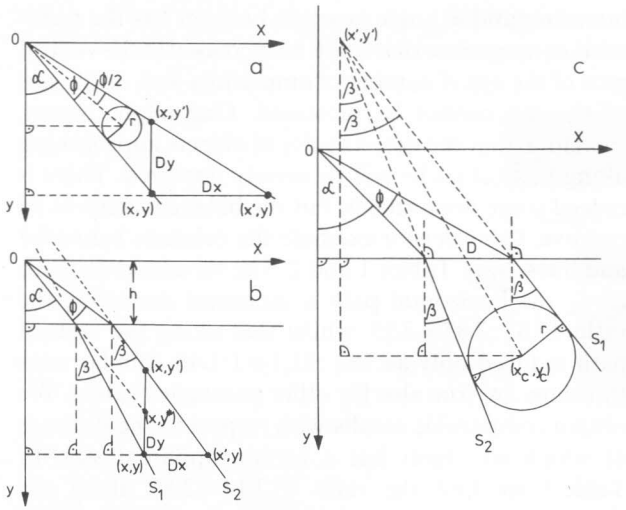

Fig. 13. **a** Definitions of symbols and geometry of rays to calculate the distances Dx, Dy in air. **b** Illustration of how α was calculated for a given pair of coordinates (x, y), and the underwater distance Dx, Dy. **c** The coordinates x', y' of the intersection of the extrapolated rays s_1, s_2, and the centre coordinates x_c, y_c of a circle to which the rays are tangent

Due to symmetry, we obtain the distance Dy by interchanging x and y in the denominator of (2):

$$\mathrm{D}y = \mathrm{tg}\,\Phi(x^2+y^2)/(x - y\,\mathrm{tg}\,\Phi)\,. \tag{3}$$

The geometry of the situation for looking into the water with an eye at height h above the surface is shown in Fig. 13b. The distance between the two rays along a horizontal line is

$$\mathrm{D}x = h\,\mathrm{tg}(\alpha+\Phi) + (y-h)\,\mathrm{tg}\,\beta' - x\,. \tag{4}$$

Since the geometry is no longer symmetrical with respect to x and y, Dy has to be calculated separately. It is

$$\mathrm{D}y = h + [x - h\,\mathrm{tg}\,\alpha]\,\mathrm{ctg}\,\beta - y'\,. \tag{5}$$

In order to calculate Dx and Dy we have to derive α for a given point (x, y). When α is calculated and Φ as well as the index of refraction n are given, β and β' can be determined. Let (x, y) be the coordinates of a point seen under the water surface (Fig. 13b). We calculate the angle α of a ray which originates in (x, y) and reaches the eye after refraction. It is

$$h\,\mathrm{tg}\,\alpha + (y-h)\,\mathrm{tg}\,\beta = x\,. \tag{6}$$

The refraction law, $\sin\alpha = n\sin\beta$, can be written as

$$\mathrm{tg}\,\beta = \sin\alpha/(n^2 - \sin^2\alpha)^{1/2}\,. \tag{7}$$

Resolving (6) and (7) results in the fourth degree equation

$$F(\mathrm{ctg}\,\alpha) = a_0 + a_1\,\mathrm{ctg}\,\alpha + a_2\,\mathrm{ctg}^2\alpha + a_3\,\mathrm{ctg}^3\alpha + a_4\,\mathrm{ctg}^4\alpha = 0 \tag{8}$$

with coefficients $a_0 = h^2(n^2-1)$; $a_1 = 2hx(n^2-1)$; $a_2 = n^2(h^2+n^2) - x^2 - (y-h)^2$; $a_3 = 2hxn^2$; $a_4 = n^2x^2$. We calculated the solution of (8) according to Newton's recursion formula:

$$(\mathrm{ctg}\,\alpha)_{i+1} = (\mathrm{ctg}\,\alpha)_i - F[(\mathrm{ctg}\,\alpha)_i]/\dot{F}[(\mathrm{ctg}\,\alpha)_i] \tag{9}$$

with $\dot{F}[\mathrm{ctg}\,\alpha] = \mathrm{d}F/\mathrm{d}(\mathrm{ctg}\,\alpha)$.

An object of length L along a horizontal line y and with its proximal end at x covers one ommatidium in air when

$$\mathrm{D}x = \mathrm{tg}\,\Phi(x^2+y^2)/(-x\,\mathrm{tg}\,\Phi + y) = L \tag{10}$$

[cf. (2)]. (10) can easily be reqritten as

$$(x + L/2)^2 + (y - L/2\,\mathrm{tg}\,\Phi)^2 = L^2(1+\mathrm{tg}\,\Phi)/4\,\mathrm{tg}^2\,\Phi\,. \tag{11}$$

Thus, the boundary line along which the object of length L covers one ommatidium is a circle with its centre at $x = -L/2$, $y = L/2\,\mathrm{tg}\,\Phi$ and radius $R = L[1+\mathrm{tg}^2\,\Phi]^{1/2}/2\,\mathrm{tg}\,\Phi$. The relationship for a vertical object of height H and its proximal end at y' is obtained by interchanging x and y in (13) and replacing L by H. The line is a circle with its centre at $x = H/2\,\mathrm{tg}\,\Phi$, $y = -H/2$ and radius $R = H[1+\mathrm{tg}^2\,\Phi]^{1/2}/2\,\mathrm{tg}\,\Phi$. If the object is a sphere with radius r and centre at x_c, y_c, the equation of the boundary line is

$$x_c^2 + y_c^2 = r^2/\sin^2(\Phi/2)\,, \tag{12}$$

as seen immediately in Fig. 13a. The line is a circle with its centre at the origin and radius $R = r/\sin(\Phi/2)$.

In order to calculate underwater boundary lines we need the equations $x_1(y)$, $x_2(y)$ of the rays s_1, s_2 corresponding to the optical axes of neighbouring ommatidia after refraction (Fig. 13b). These are

$$y_1(x) = -x\,\mathrm{ctg}\,\beta - h + h\,\mathrm{tg}\,\alpha\,\mathrm{ctg}\,\beta \tag{13}$$

$$y_2(x) = -x\,\mathrm{ctg}\,\beta' - h + h\,\mathrm{tg}(\alpha+\Phi)\,\mathrm{ctg}\,\beta' \tag{14}$$

and the inverse relationships

$$x_1(y) = -y\,\mathrm{tg}\,\beta + h(\mathrm{tg}\,\alpha - \mathrm{tg}\,\beta)\,, \tag{15}$$

$$x_2(y) = -y\,\mathrm{tg}\,\beta' + h[\mathrm{tg}(\alpha+\Phi) - \mathrm{tg}\,\beta']\,. \tag{16}$$

β and β' can be computed from α and $\alpha+\Phi$ using (7).

The y-coordinate of a horizontal object of length L with its proximal end on $x_1(y)$ covering just one ommatidium is obtained from $x_1(y) - x_1(y) = L$, which results in

$$y_h = \{L - h[\mathrm{tg}(\alpha+\Phi) - \mathrm{tg}\,\alpha]\}/(\mathrm{tg}\,\beta - \mathrm{tg}\,\beta') - h\,. \tag{17}$$

Substituting (17) in (15) we obtain the x-coordinate of the proximal end of the object, which is

$$x_h = -y_h\,\mathrm{tg}\,\beta + h[\mathrm{tg}\,\alpha - \mathrm{tg}\,\beta]\,. \tag{18}$$

Similarly, the x-coordinate of a vertical object of height H covering just one ommatidium is derived from $y_2(x) - y_1(x) = H$:

$$x_v = \{H + h[\mathrm{tg}\,\alpha\,\mathrm{ctg}\,\beta - \mathrm{tg}(\alpha+\Phi)\,\mathrm{ctg}\,\beta']\}/(\mathrm{ctg}\,\beta - \mathrm{ctg}\,\beta')\,. \tag{19}$$

The y-coordinate of the proximal end of the line is

$$y_v = -x_v\,\mathrm{ctg}\,\beta' - h[1 - \mathrm{tg}(\alpha+\Phi)\,\mathrm{ctg}\,\beta']\,. \tag{20}$$

To calculate the boundary lines for a circle of radius r which covers just one ommatidium we derive from Fig. 13c:

$D^2 = (x_c - x')^2 + (y_c - y')^2$, and $D = r/\sin[(\beta' - \beta)/2]$, i.e.

$$r^2/\sin^2[(\beta' - \beta)/2] = (x_c - x')^2 + (y_c - y')^2\,. \tag{21}$$

Furthermore, the point (x_c, y_c) lies on the line coinciding with D, the equation of which is

$$y(x) = (x_c - x')\,\mathrm{ctg}[(\beta' + \beta)/2] + y'\,, \tag{22}$$

and

$$x(y) = (y_c - y')\,\mathrm{tg}[(\beta' + \beta)/2] + x'\,. \tag{23}$$

respectively. Substituting (22) in (21) we obtain

$$x_c = x' + \{r \sin[(\beta' + \beta)/2]\}/\sin[(\beta' - \beta)/2], \quad (24)$$

and by substituting (23) in (21)

$$y_c = y' - \{r \cos[(\beta' + \beta)/2]\}/\sin[(\beta' - \beta)/2]. \quad (25)$$

The coordinates x', y' of the point at which the extrapolated refracted rays cross each other are derived from $y_1(x) = y_2(x)$ and $x_1(y) = x_2(y)$ in (13)–(16). They are

$$x' = h[\mathrm{tg}(\alpha + \Phi)\,\mathrm{tg}\beta - \mathrm{tg}\alpha\,\mathrm{tg}\beta']/(\mathrm{tg}\beta - \mathrm{tg}\beta'), \quad (26)$$

$$y' = h[\mathrm{tg}(\alpha + \Phi) - \mathrm{tg}\alpha]/(\mathrm{tg}\beta' - \mathrm{tg}\beta) + h. \quad (27)$$

Boundary lines along which an object covers more than one ommatidium are obtained by increasing Φ accordingly.

Acknowledgements. We thank H. J. Dahmen, K. Riede, and J. Zeil for valuable suggestions, for reading and correcting the manuscript. We received financial support from the Deutsche Forschungsgemeinschaft (SFB 307).

References

Dahmen HJ, Junger W (1988) Adaptation to the water surface: structural and functional specialisation of the Gerrid eye. In: Elsner N, Barth FG (eds) Sense organs. Thieme, Stuttgart New York, p 233

Günther K (1968) In: Urania Tierreich-Insekten. Urania, Leipzig Jena Berlin

Horváth G (1989) Optimization of *Notonecta's* cornea. J Theor Biol (in press)

Liche MH (1936) Beobachtungen über das Verhalten der Wasserläufer *(Gerridae, Hemiptera heteroptera).* Bull Int Acad Polon BII:525–564

Murphey RK (1971) Motor control of orientation to prey by the waterstrider *Gerris remigis.* Z Vergl Physiol 72:150–167

Murphey RK (1971) Sensory aspects of the control of orientation to prey by the waterstrider *Gerris remigis.* Z Vergl Physiol 72:169–183

Nalbach HO, Nalbach G (1987) Distribution of optokonetic sensitivity over the eye of crabs: its relation to habitat and possible role in flow-field analysis. J Comp Physiol 160:127–135

Schneider L, Langer H (1969) Die Struktur des Rhadoms im Doppelauge des Wasserläufers *Gerris lacustris.* Z Zellforsch 99:538–559

Schwind R (1980) Geometrical optics of the *Notoneca* eye: adaptations to optical environments and way of life. J Comp Physiol 140:59–68

Wohlburg-Buchholz K (1979) The organization of the lamina ganglionaris of the hemipteran insects, *Notonecta glauca, Corixa punctata* and *Gerris lacustris.* Cell Tissue Res 197:39–59

Zeil J, Nalbach G, Nalbach HO (1986) Eyes, eye stalks and the visual world of semi-terrestrial crabs. J Comp Physiol A159:801–811

Zeil J, Nalbach G, Nalbach HO (1989) Spatial vision in a flat word: optical and neural adaptions in arthropods. In: Singh RH, Strausfeld NJ (eds) Neurobiology of sensory systems. Plenum Press, New York (in press)

Received: June 19, 1989
Accepted in revised form: July 17, 1989

Prof. Dr. Dezsö Varju
Lehrstuhl für Biokybernetik
Universität Tübingen
Auf der Morgenstelle 28
D-7400 Tübingen 1
Federal Republic of Germany